Available online at www.sciencedirect.com
ScienceDirect
Computers and Geotechnics 34 (2007) 449–461
COMPUTERS AND GEOTECHNICS
www.elsevier.com/locate/compgeo

Modeling of pile installation using contact mechanics and quadratic elements

Kathrin A. Fischer, Daichao Sheng *, Andrew J. Abbo

Centre for Geotechnical and Materials Modeling, School of Engineering, The University of Newcastle, Callaghan, NSW 2308, Australia

Received 30 October 2006; received in revised form 18 January 2007
Available online 4 June 2007

Abstract

In geotechnical engineering, numerical analysis of pile capacity is often performed in such a way that piles are modeled using only the geometry of their final position in the ground and simply loaded to failure. In these analyses, the stress changes caused by the pile installation are neglected, irrespective of the installation method. For displacement piles, which are either pushed or hammered into the ground, such an approach is a very crude simplification. To model the entire installation process of displacement piles a number of additional nonlinear effects need to be considered. As the soil adjacent to the pile is displaced significantly, small deformation theory is no longer applicable and a large deformation finite element formulation is required. In addition, the continuously changing interface between the pile and the soil has to be considered. Recently, large deformation frictional contact has been used to model the pile installation and cone penetration processes. However, one significant limitation of the analysis was the use of linear elements, which have proven to be less accurate than higher order elements for nonlinear materials such as soils.

This paper presents a large deformation frictional contact formulation which can be coupled consistently with quadratic solid elements. The formulation uses the so-called mortar-type discretisation of the contact surfaces. The performance of this contact discretisation technique is demonstrated by accurately predicting the stress transfer between the pile and the soil surfaces.

Keywords: Pile installation; Large deformations; Contact mechanics; Finite elements; Cam-clay; Mortar elements

1. Introduction

Traditionally, finite element methods in geomechanics focus on finding formulations which are able to describe the complex nonlinear behaviour of soils. What is quite often overlooked is the nonlinear behaviour within the model introduced by non-smooth geometries and boundary constraints. Joint or interface elements, which are commonly utilised in geotechnical finite element simulations, can only be used properly in the context of small deformation theory. They are not appropriate for simulating pile installation or cone penetration tests that involve large deformations of the soil and also frictional sliding, separation and re-closure between the pile and the soil.

A large deformation contact formulation provides an alternative means of modeling soil-structure interfaces that undergo large relative sliding, surface separation and reclosure. Recently, Sheng et al. [15] have applied the node-to-segment element (NTS-element), based upon the work of Wriggers and Simo [23], to simulating pile installation. More recently, Sheng et al. [16] used a smooth discretisation of contact surfaces to model pile installation and oenetration. Both formulations have shown that large deformation contact formulations can successfully be used for penetration problems. However, a significant disadvantage of both formulations is that they can only be applied to linear finite elements. This is a disadvantage in soil mechanics where higher order shape functions are often used to improve accuracy and avoid locking effects.

* Corresponding author. Tel.: +61 249215746; fax: +61 249216991.
E-mail addresses: Kathrin-Anita.Fischer@gmx.de (K.A. Fischer), Daichao.Sheng@newcastle.edu.au (D. Sheng).

0266-352X/$ - see front matter © 2007 Elsevier Ltd. All rights reserved.
doi:10.1016/j.compgeo.2007.01.003

This paper presents an alternative contact formulation for large deformation formulation that is applicable to finite element meshes using high-order elements. The so-called mortar type method, presented in Fischer and Wriggers [6] originates from the domain decomposition technique where a mortar function is used to couple non-conforming meshes of arbitrary order. This discretisation technique was firstly used by mathematician such as Bernardi and Patera [1] and was first introduced to large deformation contact formulations by Puso and Laursen [14] and Fischer and Wriggers [5].

Both NTS and the mortar type formulations will be explained and the necessary variational formulations will be derived. This paper will then focus on quadratic mortar-type discretisation of the contact surfaces and the coupling with 8-noded quadrilateral soil elements. The second order discretisation already provides some smoothing of sharp corners. Such singularities, if left untreated, can lead to instable and inaccurate results like the oscillations observed in Simo and Meschke [17], Sheng et al. [16] and Fischer and Sheng [4]. In addition, a cam-clay model is used to represent the behaviour of the soil.

2. Contact mechanics

The application of contact mechanics within finite element software can be based upon either the NTS or mortar element techniques. The master–slave concept and the associated and widely used node-to-segment (NTS) discretisation is described in detail by Curnier [2] and Hallquist [7]. The papers of Fischer and Wriggers [5] and Fischer and Wriggers [6] deal with the derivation of the mortar discretisation technique for large deformation frictionless and frictional contact or further detailed derivations can be found in the textbooks of Laursen [10] and Wriggers [20]. As this paper is going to focus on their performance in pile installation processes, only a brief overview is given here about the basic idea of two different continuous contact descriptions, the incorporation in the variational formulation and finally their discretisation.

In modeling contact, one of the bodies is called the slave or non-mortar body while the other one is chosen to be the master or mortar body. The choice of master and slave body is arbitrary but has to be fixed within the set up of contact constraints. Due to the later focus on the mortar description, the bodies are named $\mathscr{B}^{nm}$ and $\mathscr{B}^{m}$, respectively. The associated contact surfaces in the initial configuration are denoted Γ^{nm} and Γ^{m}. The parametric position of an arbitrary point within these bodies is described by the variables η and ξ.

2.1. Contact kinematics

Generally, contact between two deformable bodies is described geometrically by using the so-called normal gap g_N as depicted in Fig. 1.

$$g_N := (\mathbf{x}^{nm} - \bar{\mathbf{x}}^{m}) \cdot \bar{\mathbf{n}}^{m}. \tag{1}$$

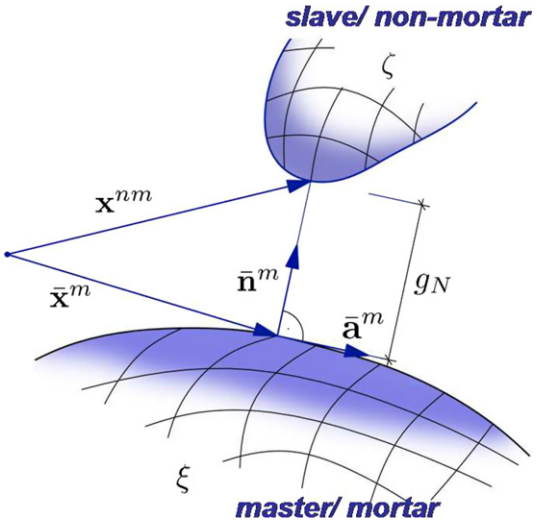

Fig. 1. Geometrical magnitudes for the contact formulation.

The normal gap gives the minimal distance between an arbitrary but fix point $\mathbf{x}^{nm}$ on the non-mortar surface and its appendant closest point projection on the mortar surface $\bar{\mathbf{x}}^{m} = \mathbf{x}^{m}(\bar{\xi}, t)$. This projection is given by the orthogonality constraint

$$(\mathbf{x}^{nm} - \bar{\mathbf{x}}^{m}) \cdot \bar{\mathbf{a}}^{m} \stackrel{!}{=} 0. \tag{2}$$

Due to the curvature of the contacting surfaces and the large deformations, this equation is nonlinear in $\bar{\xi}$ since $\bar{\mathbf{x}}^{m} = \mathbf{x}^{m}(\bar{\xi}, t)$ and $\bar{\mathbf{a}}^{m} = \mathbf{a}^{m}(\bar{\xi}, t)$. Therefore, the solution $\bar{\xi}$, which gives the closest point on the mortar surface, has to be found iteratively for the finite element discretisation of the surfaces.

Due to loading the bodies undergo large deformations. Therefore, contact has to be detected between the current configurations of the two surfaces $\gamma^{nm} = \phi_t(\Gamma^{nm})$ and $\gamma^{m} = \phi_t(\Gamma^{m})$ where ϕ_t is an operator describing the mechanical deformation between the initial and the current configuration at time t. The location of a point is the current configuration $\mathbf{x}^{i}$ (i denotes the respective body) is related to the initial configuration $\mathbf{X}^{i}$ via the total displacements $\mathbf{u}^{i}$.

$$\mathbf{x}^{i} = \mathbf{X}^{i} + \mathbf{u}^{i} \tag{3}$$

where $\mathbf{X}^{i}$ refers to the position of the point in the initial configuration.

2.2. Contact interface constraints

The area in contact between the contact surfaces changes continuously in size and position due to large deformations and relative movement of the surfaces. The detection of the current contact area $\gamma_c = \phi_t(\Gamma_c)$ is based on the evaluation of the Kuhn–Tucker conditions for non-adhesional contact for every possible contact pair $(\mathbf{x}^{nm}, \bar{\mathbf{x}}^{m})$.

$$g_N \geqslant 0, \quad t_N \leqslant 0, \quad g_N t_N = 0 \tag{4}$$

The normal stress $t_N = -p_N$ is the negative contact pressure p_N. A such, when two bodies are in contact then it is required

that $g_N = 0$. Penetration of one body into the other ($g_N < 0$) is used to indicate whether a contact constraint is meant to be established or not ($g_N > 0$). The transformation between the initial and current configuration of the contact surface is done by applying Nanson's formula.[1]

Once contact is detected between the two bodies it has to be distinguished whether they stick together or slide relatively to each other. Sticking between two bodies means that each point on the non-mortar surface has a fixed partner on the mortar surface. This connection does not change which is tantamount to $\dot{\xi} = 0$. This is similar to the fulfilment of the minimal distance (2) between the contact partners. As long as no sliding (tangential movement) between two bodies occur, the relative tangential velocity

$$\dot{\mathbf{g}}_T^{sl} = \mathscr{L}\mathbf{g}_T := \dot{g}_T^{sl}\frac{\bar{\mathbf{a}}^m}{\|\bar{\mathbf{a}}^m\|} = \dot{\xi}\bar{\mathbf{a}}^m, \qquad \dot{g}_T^{sl} = \dot{\xi}\|\bar{\mathbf{a}}^m\| \tag{6}$$

is zero. If the tangential velocity is zero, also the tangential relative displacement

$$g_T^{sl} = \int_{t_0}^{t} \|\dot{\xi}\bar{\mathbf{a}}^m\|\,\mathrm{d}t \tag{7}$$

must also be zero. This contact state is called stick case with the following restriction:

$$\text{Stick constraint} : \dot{\mathbf{g}}_T^{st} = \mathbf{0} \Longleftrightarrow \mathbf{g}_T^{st} = \mathbf{0} \tag{8}$$

A relative tangential movement between two bodies occurs if the static frictional resistance is overcome and the loading is large enough such that the sliding can occur between the two surfaces. In this paper, the frictional interface is modeled using Coulomb's law for frictional slip in its simplest form where the tangential stress $\mathbf{t}_T$ is given by

$$\|\mathbf{t}_T\| = \mu|t_N| \tag{9}$$

in which μ is the coefficient of friction.[2] The value of this coefficient depends upon the materials upon the material coming into contact with one another. The frictional stress due to friction must be exceeded for sliding between the two surfaces to occur. Therefore, the relative sliding velocity, and hence the sliding displacement, are opposite in direction to the friction force. As such the tangential stress vector is restricted as follows:

$$\text{Slip constraint} : \mathbf{t}_T^{sl} = -\mu|t_N|\frac{\dot{\mathbf{g}}_T^{sl}}{\|\dot{\mathbf{g}}_T^{sl}\|} \tag{11}$$

An indicator function

$$f = \|\mathbf{t}^{-T}\| - \mu|t_N| \tag{12}$$

has to be evaluated, which represents the Coulomb model for the frictional interface law. Using this function the two contact states can be distinguished:

$$f = \begin{cases} \|\mathbf{t}^{-T}\| - \mu|t_N| < 0 & \rightarrow \text{Stick} \\ \|\mathbf{t}^{-T}\| - \mu|t_N| = 0 & \rightarrow \text{Slip} \end{cases} \tag{13}$$

If $f = 0$ holds, the only thing which is known about the relative velocity and displacement is that $\dot{\mathbf{g}}_T^{sl} \neq \mathbf{0}$, respectively $\mathbf{g}_T^{sl} \neq \mathbf{0}$, holds. The size and direction of both just can determined by an evolution equation. The procedure to determine this evolution equation is analogous to the standard concept of elasto-plasticity theory which is given in detail in Hill [8], Prager [13] and Lubliner [11].

3. NTS-element

The contact variational formulation is set up in terms of a penalty method. The advantage of this method is that no additional degrees of freedoms, such as Lagrangeian multipliers, have to be taken into account. This fixes the size of the global system of equations and makes the iterative solution scheme more stable. Additionally, contact can be detected just by evaluating the normal gap g_N since the scalar contact stresses in the normal and tangential directions, t_N and t_T, depend linearly on the normal gap, respectively on the sliding path g_T.

$$t_N = \epsilon_N g_N \qquad t_T = \epsilon_T g_T \tag{14}$$

The penalty parameters ϵ_N and ϵ_T can be interpreted as spring stiffnesses. The virtual work is done by the compression of two springs as depicted in Fig. 2b. When penetration is detected, then a contact constraint is added between the respective contact pair and this penalises the forbidden penetration. The springs are orthogonal to each other, whereas one spring acts in normal and the other one in tangential direction. The directions are defined by the tangent and normal vector given at the point of solution $\mathbf{x}^{nm} = \bar{\mathbf{x}}^m$ with $g_N = 0$.

3.1. Variational contact formulation

The normal spring, see Fig. 2b, is squeezed by the normal stress vector $\mathbf{t}_N$ such that the virtual displacement

$$\delta g_N = (\delta\mathbf{u}^{nm} - \delta\bar{\mathbf{u}}^m)\cdot\bar{\mathbf{n}}^m \tag{15}$$

is pushed back to the solution point in the direction of $\bar{\mathbf{n}}^m$. The tangential spring is shortened by the stress vector $\mathbf{t}_T$.

[1] Nanson's Formula

$$\mathrm{d}\mathbf{a} = J\mathbf{F}^{-T}\,\mathrm{d}\mathbf{A} \tag{5}$$

$\mathrm{d}\mathbf{A} = \mathbf{N}\,\mathrm{d}A$ is the infinitesimal surface element in the initial configuration. The product of the Jacobian J, the inverse transponent of the deformation gradient $\mathbf{F}$ and $\mathrm{d}\mathbf{A}$ yields to the infinitesimal surface element $\mathrm{d}\mathbf{a} = \mathbf{n}\mathrm{d}a$ in the current configuration.

[2] $\mathbf{t}_T$ and t_N are parts of the contact stress vector $\mathbf{t}$ acting at the position $\bar{\xi}$.

$$\mathbf{t} = \mathbf{t}_N + \mathbf{t}_T = t_N\frac{\bar{\mathbf{n}}^m}{\|\bar{\mathbf{n}}^m\|} + t_T\frac{\bar{\mathbf{a}}^m}{\|\bar{\mathbf{a}}^m\|} \tag{10}$$

In the later weak formulation we are going to integrate over the initial configuration to avoid liearising the deformations of the contact area. Hence $\mathbf{t}$ results from current loading but acts on the initial configuration of the current contact surface. For this reason it has no physical meaning. Thus, $\mathbf{t}$ is a so-called pseudo stress. The transformation between this pseudo stress and the physically interpretable Cauchy stress can be easily done by applying Nanson's formula.

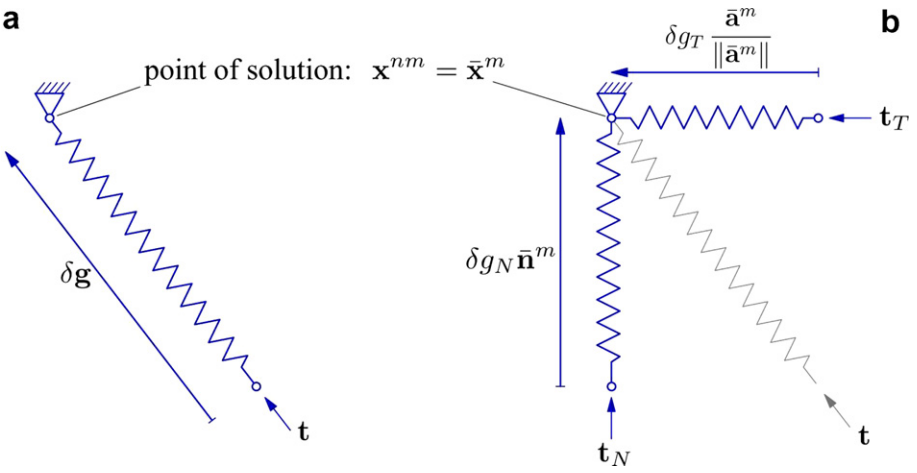

Fig. 2. Description of the virtual work: (a) in the total formulation; and (b) in the split form.

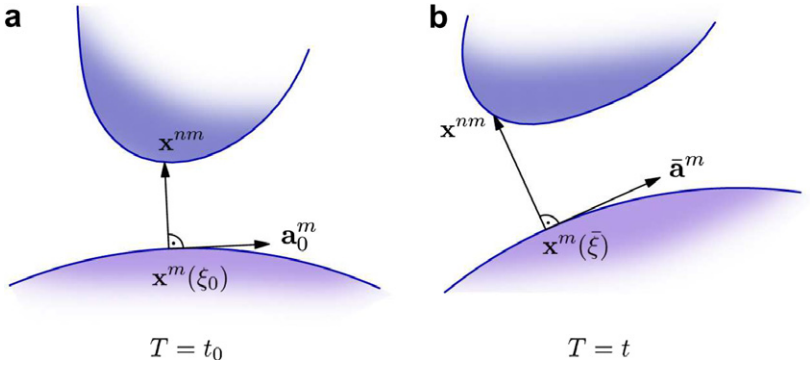

Fig. 3. Keeping the minimal distance during the sliding process at any time T.

The virtual displacement of this spring acts on the line of the tangent vector $\bar{\mathbf{a}}^m$ with δg_{T} as the virtual sliding path. With this, the split description of the contact virtual work, as call it in the following, is given by

$$G_{\mathrm{c}} := G_{\mathrm{c}}^{\mathrm{split}} = \int_{\Gamma_{\mathrm{c}}} (\delta g_{\mathrm{N}} t_{\mathrm{N}} + \delta g_{\mathrm{T}} t_{\mathrm{T}})\, \mathrm{d}A. \tag{16}$$

If tangential contact stress is transmitted at a point of solution $\mathbf{x}^{nm} = \bar{\mathbf{x}}^m$, the tangential relative displacement between $\mathbf{x}^{nm}$ and $\bar{\mathbf{x}}^m$ is zero in this direction, due to $\mathbf{g}_{\mathrm{T}}^{\mathrm{st}} = \mathbf{0} \mathbf{g}_{\mathrm{T}}^{\mathrm{st}} = \mathbf{0}$, because the contact partners stick together. As long as the tangential contact stress acts, the minimal distance (2) has to be kept at any time as depicted in Fig. 3. Therefore, the time derivative of this constraint follows as $\frac{\mathrm{d}}{\mathrm{d}t}[(\mathbf{x}^{nm} - \bar{\mathbf{x}}^m) \cdot \bar{\mathbf{a}}^m] = 0$. From this equation one obtains

$$\delta\xi = \frac{1}{\bar{a}^m - g_{\mathrm{N}} \bar{b}^m} \cdot \left[(\delta \mathbf{u}^{nm} - \delta \bar{\mathbf{u}}^m) \cdot \bar{\mathbf{a}}^m + g_{\mathrm{N}} \bar{\mathbf{n}}^m \cdot \delta \bar{\mathbf{u}}^m_{,\xi} \right] \tag{17}$$

due to equivalence between time derivative and variation.[3] In the continuum mechanical contact description the normal gap g_{N} is zero at the solution point $\mathbf{x}^{nm} = \bar{\mathbf{x}}^m$. Therefore, this equation simplifies to

$$\delta\xi = \frac{1}{\bar{a}^m} \cdot (\delta \mathbf{u}^{nm} - \delta \bar{\mathbf{u}}^m) \cdot \bar{\mathbf{a}}^m. \tag{18}$$

To determine which contact state is active, a trial step must be evaluated beforehand, in which a stick state is assumed. If Eq. $(13)_1$ holds, the trial stress is equal to t_{T}

$$t_{\mathrm{T}}^{\mathrm{st}} = t_{\mathrm{T}} = t_{\mathrm{T}}^{\mathrm{tr}} = \epsilon_{\mathrm{T}} g_{\mathrm{T}}^{\mathrm{tr}} \tag{19}$$

with the trial gap $g_{\mathrm{T}}^{\mathrm{tr}} = g_{\mathrm{T}}^{\mathrm{sl}}$. This means in terms of a penalty formulation that any possible tangential sliding will be penalised because the stick state is active. Finally it can be shown that

$$g_{\mathrm{T}}^{\mathrm{tr}} = (\xi - \xi_0) \|\bar{\mathbf{a}}^m\| \tag{20}$$

by applying $\mathrm{d}\xi = \dot{\xi}\mathrm{d}t$ and using Eq. (7). In this context the time integral starts at the time t_0, the time at which stick contact was first detected. The integral ends at the current time t. $\delta g_{\mathrm{T}}^{\mathrm{st}} = \delta g_{\mathrm{T}}^{\mathrm{tr}}$ follows from the above equation by variation.

$$\delta g_{\mathrm{T}}^{\mathrm{st}} = \delta\xi \|\bar{\mathbf{a}}^m\| + (\xi - \xi_0) \frac{\bar{\mathbf{a}}^m \cdot \delta \bar{\mathbf{a}}^m}{\|\bar{\mathbf{a}}^m\|} \tag{21}$$

If Eq. $(13)_1$ does not hold, the tangential stress stems from the constitutive law for frictional slip as mentioned in Eq. (11). From this equation we obtain

$$t_{\mathrm{T}}^{\mathrm{sl}} = t_{\mathrm{T}} = -\mu |t_{\mathrm{N}}| \mathrm{sign}(g_{\mathrm{T}}^{\mathrm{tr}}). \tag{22}$$

[3] In this paper $(\ldots)_{,\xi}$ shortens the expression $\frac{\mathrm{d}}{\mathrm{d}\xi}(\ldots)$. The same holds for $(\ldots)_{,\xi\xi} = \frac{\mathrm{d}^2}{\mathrm{d}\xi^2}(\ldots)$. Furthermore, $\bar{a}^m = \bar{\mathbf{a}}^m \cdot \bar{\mathbf{a}}^m$ is the metric and $\bar{b}^m = \bar{\mathbf{x}}^m_{,\xi\xi} \cdot \bar{\mathbf{n}}^m$ is the curvature.

The starting point of $\delta g_{\mathrm{T}} = \delta g_{\mathrm{T}}^{\mathrm{sl}}$ moves from ξ_0 at time t_0 to $\tilde{\xi}_0$. Eq. (22) can be used to derive and expression for the new position $\tilde{\xi}_0$ for the next trial step.

$$(\xi - \tilde{\xi}_0)\|\bar{\mathbf{a}}^m\| = -\frac{\mu}{\epsilon_{\mathrm{T}}}|t_{\mathrm{N}}|\mathrm{sign}(g_{\mathrm{T}}^{\mathrm{tr}}) \tag{23}$$

The variation of the tangential gap

$$\delta g_{\mathrm{T}}^{\mathrm{sl}} = \delta\xi\|\bar{\mathbf{a}}^m\| \tag{24}$$

results directly from the Lie derivative $(6)_2$ using the equivalence between the time derivative and the variation. The associated tangential slip is given in (7).

Since the update of the coordinate $\xi_0 \to \tilde{\xi}_0$ as well as the integration of the friction law must be consistent to the chosen discretisation, its derivation has to be taken carefully into account. Interested readers can find further information in Wriggers [19].

With this, Eq. (16) can be split in two equations for stick and slip case. By inserting (19) and (21), the virtual work for stick follows as

$$G_{\mathrm{c}}^{\mathrm{st}} = \int_{\Gamma_{\mathrm{c}}} \left(\delta g_{\mathrm{N}} t_{\mathrm{N}} + \delta g_{\mathrm{T}}^{\mathrm{st}} t_{\mathrm{T}}^{\mathrm{st}}\right) \mathrm{d}A. \tag{25}$$

Accordingly, with Eqs. (24) and (22) the virtual work for slip is given by

$$G_{\mathrm{c}}^{\mathrm{sl}} = \int_{\Gamma_{\mathrm{c}}} \left(\delta g_{\mathrm{N}} t_{\mathrm{N}} + \delta g_{\mathrm{T}}^{\mathrm{sl}} t_{\mathrm{T}}^{\mathrm{sl}}\right) \mathrm{d}A. \tag{26}$$

Finally, the contact virtual work $G_{\mathrm{c}}^{\mathrm{st/sl}}$ has to be added to the variational formulation of the entire problem describing the equilibrium between the internal and external virtual work of non-mortar and mortar body including the connecting contact constraints.

$$G = \left(G^{nm} + G^{m}\right)_{int} + \left(G^{nm} + G^{m}\right)_{\mathrm{ext}} + G \overset{!}{=} 0 \tag{27}$$

3.2. Finite element discretisation

Once the variational form has been obtained, it can be approximated by a finite element discretisation using shape functions.

$$G_{\mathrm{c}} \approx G_{\mathrm{c}}^{h} = \int_{\Gamma_{\mathrm{c}}^{h}} \left(\delta g_{\mathrm{N}}^{h} t_{N}^{h} + \delta g_{\mathrm{T}}^{h} t_{\mathrm{T}}^{h}\right) \mathrm{d}A^{h} \tag{28}$$

Again, further details in relation to this can be found in Wriggers [20] or Wriggers [18], where the whole linearisation procedure and the associated finite element discretisation is derived in detail. This paper only presents basic idea behind the NTS-element in order to understand the difference with the mortar type approach introduced later in this paper.

The idea of the node-to-segment element is that the integral over the entire discrete contact surface Γ_{c}^{h} is substituted by a sum over all slave nodes n_{c} which are currently in contact

$$G_{\mathrm{c}}^{h} = \sum_{s=1}^{n_{\mathrm{c}}} \left(\epsilon_{\mathrm{N}} \delta g_{N_s} g_{N_s} A_s + \delta g_{T_s} t_{T_s} A_s\right) \tag{29}$$

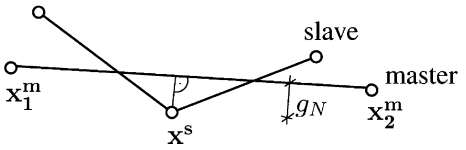

Fig. 4. Node-to-segment (NTS-) element.

where A_s is the area around each slave node s. This means that whenever a slave node, as depicted in Fig. 4, penetrates a master element, a contact constraint at this certain slave node is added to the entire problem. This so-called colliquation method includes a strong or nodal projection of the contact constraints whereby every single nodal contact constraint is treated equally. This can be done as long as linear shape functions are used because then the weighting of every contact constraint is the same. Therefore, this discretisation technique is only applicable in combination with linear shape functions. The coupling of the NTS-element formulation with higher order discretisations of the joint solids would lead to inconsistencies in the stress transfer. This is due to the weighting of the slave node contributions which would not be equal anymore. In this case, the correct weightings can only be evaluated by evaluating the integral exactly. This restricts the usability for soil mechanics since the NTS-element can only be combined with simple soil models. More complex soil models need to be discretised by higher order shape functions. Therefore, they cannot be used in combination with this contact discretisation.

3.3. Performance of NTS-element

The performance of the NTS-element contact formulation was investigated by simulating the installation of a pile. This analysis is similar to that performed by Sheng et al. [16]. In these analyses quadrilateral 4-nodal-axis-symmetric elements are used to model both the soil and the pile, see 5. Symmetry of the problem is exploited to simplify the computation and to reduce the number of degrees of freedom. The soil is modeled using a modified cam-clay model. The properties of the soil are such that slope of the normal compression line λ and the slope for the unloading–reloading line κ decrease gradually between the ground surface and the depth of 17 m. The pile is treated as a stiff elastic material with Young's modulus and Poison's ratio as given in the figure. For the contact discretisation the lateral soil surface is chosen to be the slave surface while the outward surface of the pile is selected as the master. Provided linear shape functions are used, the NTS-element discretisation can be coupled consistently with soil elements. The contact formulations described in this paper have been implemented with *SNAC* which is a finite element code is developed at the University of Newcastle to solve nonlinear geotechnical problems, see *SNAC* Handbuch. All simulation presented in this paper have been performed using this software.

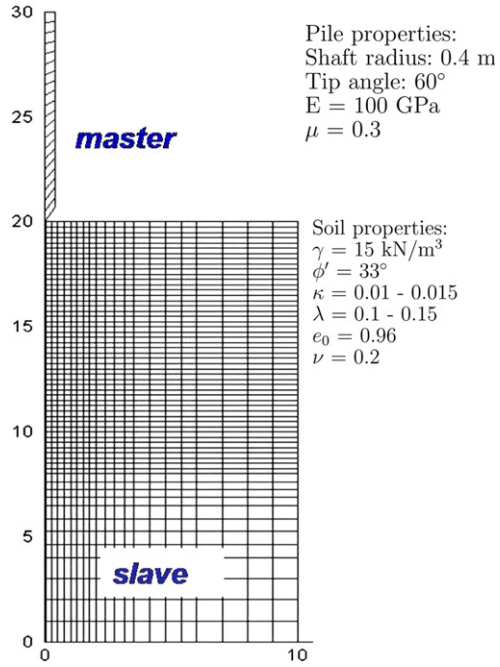

Fig. 5. Mesh and material parameters.

The simulation starts with the pile located above the ground surface. Gravity loading is then applied to establish the initial stresses within the soil. Once these have been computed the void ratio is set to a given value e_0. The pile is then pushed into the soil to a depth of 6 m by prescribing the displacements at its top boundary.

The results of this analysis is a load–displacement plot that plots the total resistance, or vertical reaction, against the penetration of the pile. As shown in Fig. 6, the general trend of the curve shows the expected behaviour. As the pile penetrates further into the soil, resulting in increased friction between pile and soil, the total resistance increases. However, the oscillations within each curve, do not reflect real behaviour. Even if sudden drops of the resistance can be observed in in situ tests, the periodical zig-zagging cannot be explained by that. While drops do happen in reality, this stems from cracking and fracturing which are not included in this finite element model. The observed oscillations in the simulation stem from the NTS-discretisation. Whenever a slave (soil) node comes close to the transition point between the pile tip and the shaft due to further downward movement, the associated soil element gets badly distorted. Then, the node turns suddenly around the transition point. Hence a sudden change of contact stress directions takes place. This comes along with a sudden drop of the vertical reaction, as Fig. 7 explains. The vertical reaction increases again with further downward movement of the pile until the next slave node comes turns around.

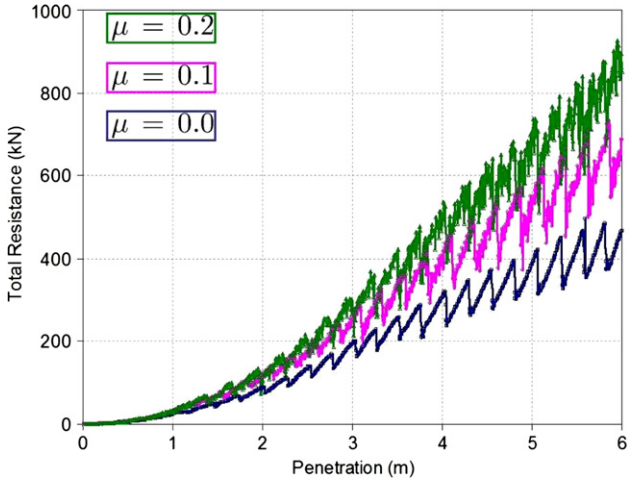

Fig. 6. Vertical reaction of the pile versus penetration with NTS-discretisation.

One possible strategy to overcome this is to consider mesh refinement. But a sharp corner represents a non-smooth boundary constraint which leads to infinite stresses and high distortions in the soil. Thus, by refining the mesh of the soil, the singularity gets even worse. This can even lead to divergence of the entire finite element simulation. Since the discretisation of a non-smooth geometry causes the oscillations, other contact discretisation techniques should be taken into account in order to obtain better stress distributions on the contact interface.

4. Mortar type method

The NTS-formulation is based on a split formulation in which the normal and tangential components are considered separately, see Eq. (16). In contrast the mortar approach is formulated by considering the total virtual work.

$$G_c := G_c^{\text{total}} = \int_{\Gamma_c} (\delta \mathbf{u}^{nm} - \delta \bar{\mathbf{u}}^{m}) \cdot \mathbf{t} \, dA \tag{30}$$

This equation is equal for both contact states (stick and slip) as long as the contact stress $\mathbf{t}$ includes the respective constraints. The variational terms are merged by the variational gap vector

$$\delta \mathbf{g} = \delta \mathbf{u}^{nm} - \delta \bar{\mathbf{u}}^{m}. \tag{31}$$

An illustration of the contact virtual work (30) is given in Fig. 2a. The point of solution is the point where the contacting bodies transmit stresses between each other. This point is virtually displaced by $-\delta \mathbf{g}$. The quantity of this displacement corresponds to the length of a virtual spring in its rest position which is attached to the point of solution. Contact virtual work is performed if the spring is totally squeezed by a stress vector $\mathbf{t}$. This means that the total stress vector $\mathbf{t}$ acts in the line of action of an imagined spring, whereas $\mathbf{t}$ must have the same direction as the displacement $\delta \mathbf{g}$. The point of solution is fixed during deformation as long as stick is assumed between the two points. If stick changes to slip state, the connection breaks and a new contact partner $\bar{\mathbf{x}}^m$ has to be found for $\mathbf{x}^{nm}$. The

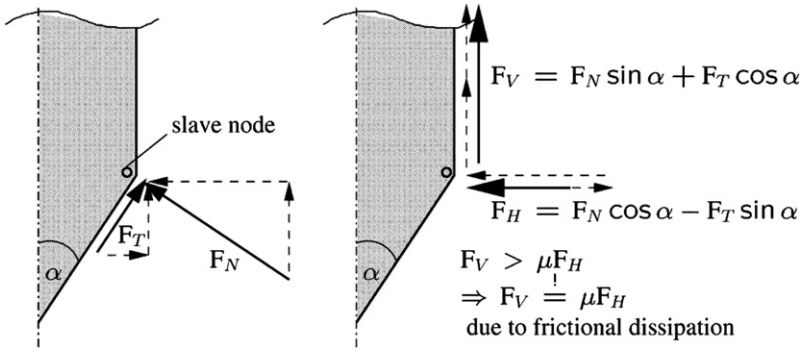

Fig. 7. Rearrangement of stresses at the sharp corner.

virtual work of the new contact pair (point of solution) can again be described by a (new) spring.

For stick, the total contact stress vector is represented by

$$\mathbf{t}^{\mathrm{st}} = \epsilon \mathbf{g}^{\mathrm{st}} \tag{32}$$

where ϵ represents the spring stiffness in total direction. The gap vector is associated to the difference vector between a fixed point $\mathbf{x}^{nm}$ on the non-mortar surface and a fixed point $\bar{\mathbf{x}}^{m}$ on the mortar surface. As long as stick state is assumed, the gap vector is

$$\mathbf{g}^{\mathrm{st}} = \mathbf{g}^{\mathrm{st}}_{n+1} = \mathbf{x}^{nm}_{n+1} - \mathbf{x}^{m}_{n+1}(\bar{\xi}_n) \tag{33}$$

for the current time t_{n+1} acting at the fixed position $\bar{\xi}_n$. Hence, one obtains

$$G^{\mathrm{st}}_{\mathrm{c}} = \int_{\Gamma_{\mathrm{c}}} \epsilon \delta \mathbf{g}^{\mathrm{st}} \cdot \mathbf{g}^{\mathrm{st}} \, \mathrm{d}A \tag{34}$$

with the variational gap vector

$$\delta \mathbf{g}^{\mathrm{st}} = \delta \mathbf{g}^{\mathrm{st}}_{n+1} = \delta \mathbf{u}^{nm}_{n+1} - \delta \mathbf{u}^{m}_{n+1}(\bar{\xi}_n). \tag{35}$$

For slip, the contact stress vector incorporates the constitutive law for frictional slip which holds in tangential direction. Therefore, the total stress vector can either be split in normal and tangential parts, as done in Section 3.1, or as presented here, given in total direction.

$$G^{\mathrm{sl}}_{\mathrm{c}} = \int_{\Gamma_{\mathrm{c}}} \delta \mathbf{g}^{\mathrm{sl}} \cdot \mathbf{t}^{\mathrm{sl}} \, \mathrm{d}A \tag{36}$$

With Eq. (10), the sliding velocity (6) and the slip constraint (11), the total stress due to sliding can be expressed by

$$\begin{aligned} \mathbf{t}^{\mathrm{sl}} := \mathbf{t} &= t_{\mathrm{N}} \bar{\mathbf{n}}^{m} - \mu |t_{\mathrm{N}}| \mathrm{sign}(\dot{\xi}) \frac{\bar{\mathbf{a}}^{m}}{\|\bar{\mathbf{a}}^{m}\|} \, [2ex] \\ &= t_{\mathrm{N}} \left[\bar{\mathbf{n}}^{m} + \mu \mathrm{sign}(t_{\mathrm{N}}) \mathrm{sign}(t_{\mathrm{T}}) \frac{\bar{\mathbf{a}}^{m}}{\|\bar{\mathbf{a}}^{m}\|} \right] \end{aligned} \tag{37}$$

Since the direction of sliding is opposite to the direction of the frictional stress, $\mathrm{sign}(\dot{\xi}) = -\mathrm{sign}(t_{\mathrm{T}})$ holds. The vector $\mathbf{g}_{\perp}$ is depicted in 8b (for $s_{\mathrm{N}} = s_{\mathrm{T}} = 1$) as

$$\mathbf{g}_{\perp} = \bar{\mathbf{a}}^{m} - \mu s_{\mathrm{N}} s_{\mathrm{T}} \bar{\mathbf{n}}^{m} \|\bar{\mathbf{a}}^{m}\|. \tag{38}$$

The total moving direction is given by the constitutive equation for friction which is restricted to Coulomb's law and friction coefficient μ. s_{N} and s_{T} correspond to the signum-functions of the normal stress and the tangential stress, evaluated at $\bar{\xi}$.

$$\begin{aligned} s_{\mathrm{N}} &= \mathrm{sign}(t_{\mathrm{N}}) \\ s_{\mathrm{T}} &= \mathrm{sign}(t_{\mathrm{T}}) \end{aligned} \tag{39}$$

Due to the initialisation of sliding, the contact partner of $\mathbf{x}^{nm}_{n+1}$ changes from $\mathbf{x}^{m}_{n+1}(\bar{\xi}_n)$ to a new position $\mathbf{x}^{m}_{n+1}(\bar{\xi}_{n+1})$ which is then assumed to be fix again. Hence the variational gap vector follows as

$$\delta \mathbf{g}^{\mathrm{sl}} = \delta \mathbf{g}^{\mathrm{sl}}_{n+1} = \delta \mathbf{u}^{nm}_{n+1} - \delta \mathbf{u}^{m}_{n+1}(\bar{\xi}_{n+1}) \tag{40}$$

The update $\bar{\xi}_n \to \bar{\xi}_{n+1}$ is based on a formulation in terms of the direction of the total stress vector (10), which matches

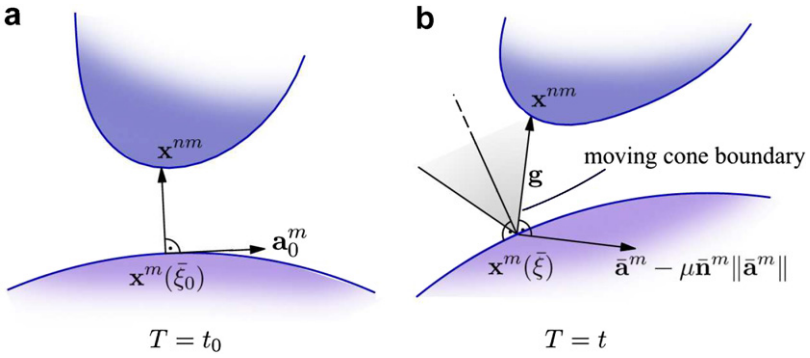

Fig. 8. Movement of ξ with the friction cone: (a) initial configuration; (b) current configuration.

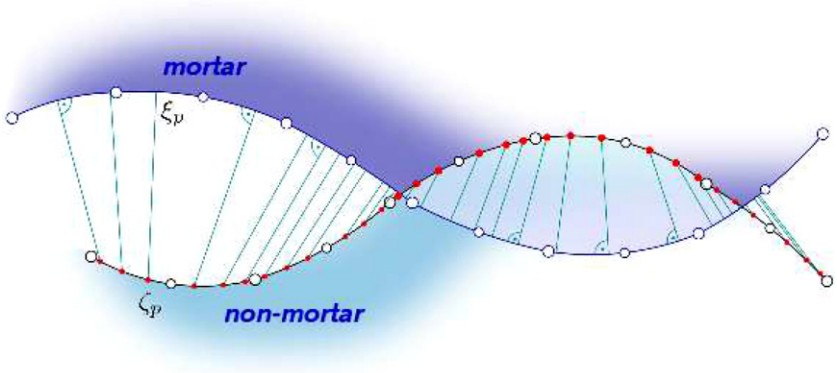

Fig. 9. Mortar type element discretisation.

consistently with the total variational formulation as given in Eq. (30). It is important to mention that, using this projection method, ξ_n changes due to sliding but not in stick case. As Fig. 8a shows, the gap vector is perpendicular to the mortar surface in the initial configuration. Since this projection method does not necessarily keep the minimal distance between the contact partners at any time, the direction of $\mathbf{g}$ can change. In case of sliding, $\mathbf{g}$ has the same inclination as the cone boundary, representing the friction law, see Fig. 8b. Thus, this projection method is called moving cone description, see [21]. Since the whole load is transferred via the direction of the total stress, a relative movement can only take place in the orthogonal direction. This moving direction $\mathbf{g}_\perp$ can be derived from the orthogonality condition

$$\mathbf{t}^{\mathrm{sl}} \cdot \mathbf{g}_\perp \stackrel{!}{=} 0. \tag{41}$$

As a result of the parallelism between the total stress vector and $\mathbf{g}$, the time derivative of the orthogonality constraint yields

$$\frac{\mathrm{d}}{\mathrm{d}t}\left[(\mathbf{x}^{nm} - \bar{\mathbf{x}}^m) \cdot (\bar{\mathbf{a}}^m - \mu s_{\mathrm{N}} s_{\mathrm{T}} \bar{\mathbf{n}}^m \|\bar{\mathbf{a}}^m\|)\right] = 0. \tag{42}$$

This equation is used to derive the update of $\bar{\xi}_n \to \bar{\xi}_{n+1}$ due to sliding.[4]

Finally, the variational formulation indicating the accordant contact state has to be included in the entire weak formulation (27) of the mechanical problem which is to be solved. This derivation in this paper provides the base for the finite element discretisation in terms of the mortar type element. For a further detailed explanation of the iterative update and the mortar type approach itself refer to Fischer and Wriggers [6].

[4] In comparison to that, Eq. (23) is used for the update in regards to the NTS-formulation. Herein, it is already assumed that the contact surface is straight in sections with respect to the later linear discretisation. Since the mortar type formulation can be applied with higher order discretisations, the update is hold more general. Thus, the nonlinear equation (42) must be solved iteratively.

4.1. Finite element discretisation

The main difference between the NTS-formulation and the mortar approach is the different approximation of the integrand Γ_{c}^h according to Eq. (28). Whilst the NTS-discretisation includes a strong or nodal projection of the contact constraints, see Eq. (29), the original mortar method fulfils the contact constraints at an interface, see [14]. Therefore, overlapping regions between the discretised contact surfaces have to be determined and within each overlapping region a numerical integration is applied. This mesh tying procedure is rather expensive and so the original method has been adopted. This so-called mortar type method differs in that overlapping regions are not detected. Instead, the integration is approximated by a sum over a fix number of Gauss points within each non-mortar segment, see Fig. 9. Hence the contact constraints are projected weakly or point wise according to their weightings. Both surfaces are discretised with quadratic shape functions. At each Gauss point p the gap vector is evaluated between $\mathbf{x}^{nm}(\zeta_p)$ and its accordant projection $\mathbf{x}^m(\xi_p)$. The associated projection method includes an iterative solution procedure since the discretisation of Eqs. (2) and (42) with quadratic shape functions leads to nonlinear projections in terms of ξ_p. Fig. 9 shows as well that every position vector $\mathbf{x}^{nm}(\zeta_p)$ can be projected to another mortar segment. This leads to a non-smooth normal gap and stress distribution. Since Gauss quadrature can only solve smooth function exactly, the application of this numerical integration yields to an approximate solution. But Fischer and Wriggers [5] have shown that the higher the number of Gauss points is, the better the integral of this non-smooth function can be approximated. For the pile installation problem 10 Gauss points per non-mortar segment seem to be absolutely sufficient if the advantages of this method are exploited.

The benefit of this approach is that even if a lot of Gauss points are used, the computational effort is a lot less expensive since overlapping regions must not be detected. Especially for large deformation problems like pile-installation where the size and position of contact partners changes massively during the simulation this is a big advantage.

The transfer from the weak formulation (30) to a discretised form by using Gauss quadrature works as follows:

A function $f = f(\zeta,\xi)$ is given which represents the contact constraint for either slip or stick state. The integral expression is approximated by

$$\begin{aligned} G_{\mathrm{c}} &= \int_{\Gamma_c} f(\zeta,\xi)dA \approx G_{\mathrm{c}}^{h} = \bigcup_{e=1}^{M} \int_{\Gamma_{\mathrm{c}}^{e}} f_e(\zeta,\xi)\,\mathrm{d}A_{\mathrm{c}}^{e} \\ &= \bigcup_{e=1}^{M} \int_{-1}^{+1} f_e(\zeta,\xi)\|\mathbf{a}_{0e}^{nm}\|\,\mathrm{d}\zeta \\ &\approx \bigcup_{e=1}^{M} \sum_{p=1}^{N} f_e(\zeta_p,\xi_p)\cdot\|\mathbf{a}_{0e_p}^{nm}\|\cdot w_p. \end{aligned} \tag{43}$$

Herein, N denotes the number of all Gauss points belonging to one mortar element e within all active mortar elements M. One mortar type element consists of all active contact pairings between one single non-mortar segment and its associated projections to the appendant mortar segments. w_p is the weighting related to each Gauss point. $\|\mathbf{a}_{0e_p}^{nm}\|$ which represents $\mathrm{d}\zeta$ is the absolute value of the tangent vector evaluated at ζ_p in the initial configuration.

Active Gauss points within a mortar type element are determined by the check of the normal traction, respectively, the normal gap at each integration point. If

$$g_{Ne_p} \leqslant 0 \tag{44}$$

is fulfilled, point p within mortar element e is added to the active contact set, otherwise not. The active contact surface is detected in the current configuration by means of an active set strategy, see [12]. Therefore, the current contact surface γ_{c} is updated before each incremental solution step. Afterwards it is translated in terms of the initial configuration with Nanson's formula.

Then, the contact state and each pair (ζ,ξ) are evaluated by a trial step which assumes stick state. If stick state is active, the pair which was initially found by the minimal distance projection, sticks together. If slip state is active, the pair has to be redefined by the moving cone projection and the contact constraint has to be changed into slip state.

The matrix notation and iterative solution schemes which are part of the finite element contact formulation including discretisations and linearisations can be taken over from Fischer and Wriggers [6]. Readers who are interested in the entire complexity of the mortar type formulation including its origin, its idea, the variational formulation, the discretisation and the solution algorithm, should refer to Fischer [3].

4.2. Performance of improved pile–soil finite element model

The simulation of the installation of a pile was modeled using mortar elements. The modeling of the pile, using linear elements, required the pile tip and the shaft of the pile to be modeled as straight surfaces, see Fig. 10a. The use of the mortar type method as the finite element contact model allowed curvature to be included in the surface elements due to quadratic shape functions. The finite element discretisation of the pile was refined in order to remove the sharp corner as depicted in Fig. 10b. Two simulations of the pile were performed; the first modeling the pile as two straight surfaces and the second incorporating the smoothed corner. In both case the solid elements were discretised by 8-nodal-quad elements. The simulation using straight surfaces produced vertical reactions that exhibit an oscillating distribution as depicted in Fig. 11. Two distinct kinds of oscillations can be observed in this plot and these can be split into first and second order oscillations. The first order oscillations have the longer wavelength of approximately 0.5 m. The second order oscillations are superposed over the first order ones and have a much smaller wave length and amplitude. As the pile is driven into the soil, elements below the tip are displaced such that it flows from in front of the tip, around the corner of the pile and along the shaft. As the soil element passes over the corner it becomes highly compressed and distorted and then it turns around the corner or transition point. Such a soil element in the stage of switching from being in front of the tip to being adjacent to the shaft is drawn to a larger scale in Fig. 12a. This transition is directly connected to the first order oscillations as the wave length of the oscillation are equal to the side length of the soil elements passing the corner. The magnitude of the wave grows as the soil element is compressed in front of the tip. The peak magnitude is reached when the element makes the transition around the corner.[5] This indicates that as long as the corner is modeled as a sharp transition

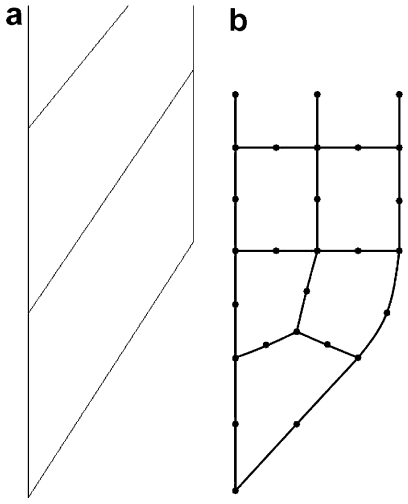

Fig. 10. Corner geometry and mesh: (a) sharp corner; (b) smoothed corner.

[5] This computation was done by using 30 Gauss point per non-mortar segment. By using less quadrature points the curve becomes smoother because the second order oscillations are picked roughly; they become refined by increasing the number of quadrature points.

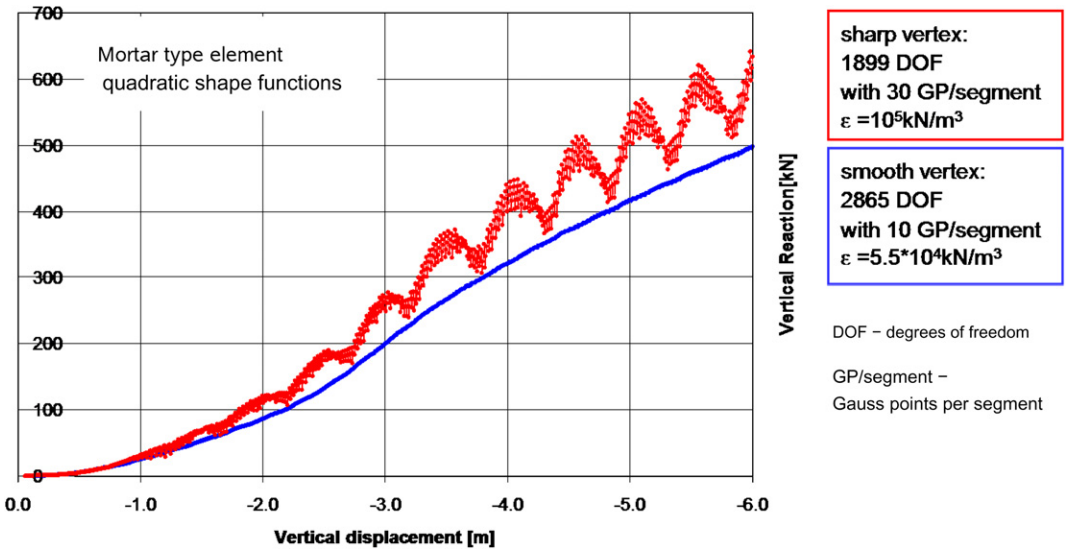

Fig. 11. Vertical reaction versus penetration with mortar type discretisation for sharp and smooth corner.

there will be oscillating reactions no matter which contact discretisation is used.

The second simulation exploits the benefits of the mortar type method by using quadratic shape functions to round the corner of the pile. Although the geometry is slightly different to that used in the first simulation, this change is more realistic since a load transfer at sharp corners or non-smooth geometries is, in general, a singularity which leads to infinite stresses and high distortions. Indeed, such a perfect sharp corner would not exist due to abrasion, for instance.

The results of the smooth model are compared to the results of the sharp corner in Fig. 11. The smoothing of the geometry leads to a smooth distribution of the vertical reaction. The plot also confirms that the geometry change does not effect the results a lot. In fact, the smooth curve runs along the bottom border of the oscillating curve. Since the upper peaks stem from the singular behaviour, which cannot be interpreted mechanically, the smoothed curve and therefore the lower bound of the other curve represent the correct distribution. The little difference between both is due to different penalty parameters. The associated deformed meshes around the transition point are shown in Fig. 12b. The visible penetration is due to the penalty method. Its magnitude can be adjusted by the penalty parameter. Choosing an acceptable penalty parameter is delicate and requires some of the user's experience due to contact simulation. Thus, the following section is dedicated to the use and influence of the penalty parameter.

Also, oscillations within the frictional NTS-discretisation, shown in Fig. 6, can also be overcome by applying the mortar type discretisation. Referring to Fig. 13 all curves depending on different friction coefficients are smooth and lie in the same range as the results of the NTS-model.

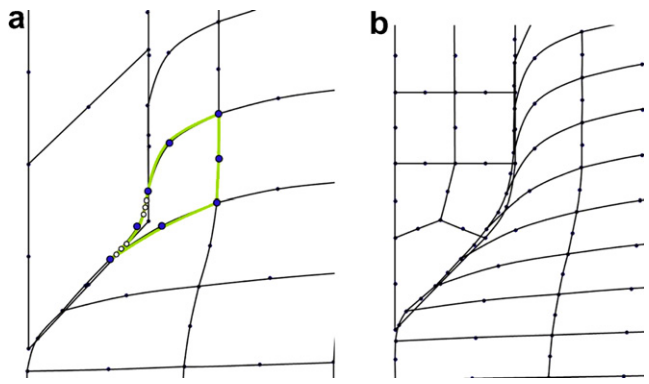

Fig. 12. Deformed mesh due to: (a) the sharp pile corner; and (b) smooth corner.

4.3. Dependance on the penalty parameter

One can show that the solution of the penalty formulation converges to the exact solution, if $\epsilon \to \infty$, see [12] and [9]. Due to ill-conditioning of the global equation system, ϵ cannot be chosen arbitrarily high. Hence the side constraint $\mathbf{x}^{nm} - \bar{\mathbf{x}}^{m} \stackrel{!}{=} 0$ on Γ_c cannot be fulfilled exactly and a penetration rests in the contact area. In general, the penalty parameter can be interpreted as a continuous bedding within the contact area; the higher the penalty factor is, the stiffer the bedding acts and therefore the penetration becomes small. If the penalty parameter is small, the bedding acts softly. Hence a large penetration must be taken into account which does not satisfy the physical contact constraint. Despite the adaptation of the penalty factor to the particular contact problem, the penalty formulation has the advantage that it is purely geometrically based and therefore no additional degrees of freedom must be activated or deactivated.

These general facts have to be taken into account to find an optimal penalty parameter ϵ_{opt} which suits the pile-installation problem in order to achieve the best possible

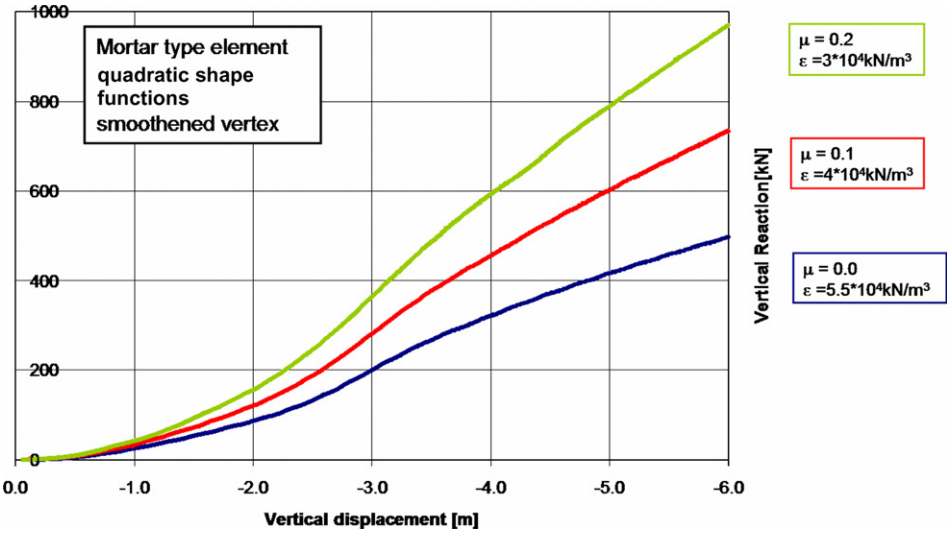

Fig. 13. Frictional vertical reaction versus penetration with mortar type element and smoothed corner.

results. A general applicable mathematical procedure is not available for finding ϵ_{opt} since the correct choice depends strongly nonlinear on the problem's properties including e.g. material descriptions and boundary constraints.

So, it is more the user's task to decide which choice is acceptable and yields to adequate results.

For the presented frictionless example the parameters $\epsilon = 5.5 \times 10^4$ kN/m^3 were chosen. This choice is based on several computations to obtain an upper and lower threshold for ϵ. The vertical reactions by applying these thresholds are depicted in Fig. 14. One can see that the chosen penalty parameter lies enclosed and leads to a smooth distribution of the vertical reaction. The associated penetration between the pile and the soil, see Fig. 15, is negligible with regards to the entire dimension of the problem.

The range between the upper and lower threshold is large. However, the best solution can be found close to the upper threshold because the higher the penalty parameter, the better the physical problem is reflected. It is not possible to obtain any convergence above the upper threshold of 10^6 kN/m^3 due to ill-conditioning. Although the penetration in these areas is nearly invisible, as Fig. 15b shows, the ill-conditioning is literally visible in Fig. 14.

The curve for the upper threshold starts to oscillate smoothly (due to a smooth pile tip model) after the entire pile tip is pushed into the ground. Then, the amplitude increases with further installation. This behaviour is directly correlated to the increase of the number of contact constraints since every contact constraint is described by using this high penalty parameter. If the parameter is high, the ill-conditioning gets worse with the number of active constraints. The wave length correlates with the length of the soil elements (0.25 m) which are passing the transition point. Even if the transition point is discretised smoothly,

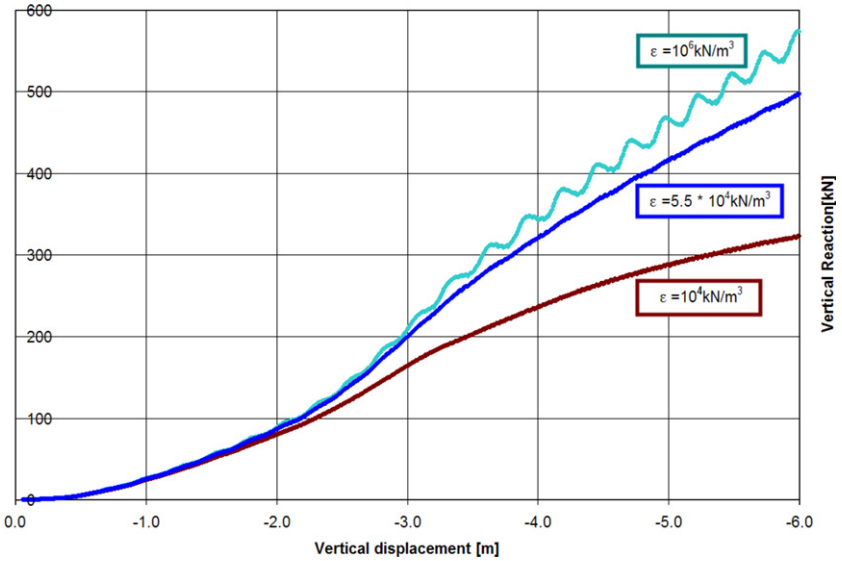

Fig. 14. Dependance of the vertical reaction on the penalty parameter.

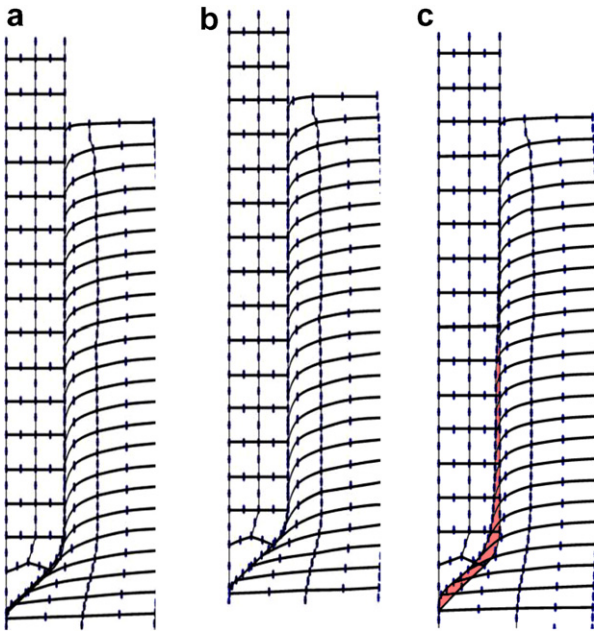

Fig. 15. Deformed mesh for: (a) $\epsilon = 5.5 \times 10^4$ kN/m^3; (b) $\epsilon = 10^6$ kN/m^3; and (c) $\epsilon = 10^4$ kN/m^3.

oscillations are visible because of a high penalty parameter which stiffens up the contact area. Therefore, every unevenness in the discrete model becomes visible.

The lower threshold is found for $\epsilon = 10^4$ kN/m^3. It is defined subjectively by looking at the deformations depicted in Fig. 15c. The physical problem seems to be badly treated since the penetrations around the pile tip are very large. However, the problem is well conditioned and the computation is absolutely stable.

In general, an acceptable penalty parameter should lead to a stable, well-conditioned global equation system. Therefore, the penalty parameter must not be too high. However, it should be chosen as high as possible, as long as the results are smooth and do not start to reflect unevenness resulting from the discretisation.

5. Conclusions

The NTS-element is commonly used to discretise the contact surfaces in large deformation contact problems. This approach contains a strong or nodal projection of the displacements. This means that the contact stress distribution is highly dependent upon the surface discretisation. This is especially true when modeling non-smooth geometric parts such as the angular corner between the tip and the shaft of a pile. Additionally, the NTS-element can only be coupled consistently with linearly discretised solid elements. This restricts the applicability of the NTS-element to soil mechanics since complex soil models have to be discretised with higher order elements to avoid locking effects and to improve accuracy. In contrast to this, the mortar approach contains a weak projection of the contact constraints. This enables this contact discretisation to be coupled consistently with higher order elements because this formulation includes a general integration scheme over the entire contact area.

Applying the mortar type element to the pile–soil problem, can lead to two basic advantageous effects. Firstly, this contact element can be coupled consistently with higher order soil elements. Secondly, non-smooth boundary constraints like the transition point can be smoothed. This finally leads to smooth solutions which depend much less on the discretisation and reflect much better the contact interaction of real pile installation problems.

The finite element model presented in this paper is subject to ongoing development to improve the modeling of other complex problems in soil mechanics. One area to be considered is due to the very large deformations in the soil. Such deformations can result in the soil mesh becoming highly distorted which in turn often leads to unstable solutions. Future work will focus on the combination of the presented large deformation finite element formulation including contact with automatic mesh refinement, like an arbitrary Lagrangeian–Eulerian (ALE-) techniques to address such issues.

References

[1] Bernardi C, Patera A. Domain decomposition by the mortar element method. Asymptotic and numerical methods for partial differential equations with critical parameters. Netherlands: Kluwer Academic Publishers; 1993. p. 269–86.
[2] Curnier A. A theory of friction. Int J Solids Struct 1984;20:637–47.
[3] Fischer KA. Mortar type methods applied to nonlinear contact mechanics. Ph.D. thesis. Institut für Baumechanik und numerische Mechanik. Germany: Universität Hannover; 2005.
[4] Fischer KA, Sheng D. Different aspects on large deformation contact formulations applied to pile–soil FE-analysis. In: Schweiger H, editor. Numerical methods in geotechnical engineering; Taylor & Francis Group, London. Sixth European conference on numerical methods in geotechnical engineering (NUMGE6), Graz, Austria, 2006. p. 613–18.
[5] Fischer KA, Wriggers P. Frictionless 2D contact formulations for finite deformations based on the mortar method. Comput Mech 2005;36:226–44.
[6] Fischer KA, Wriggers P. Mortar based frictional contact formulation for higher order interpolations using the moving friction cone. Comput Methods Appl Mech Engng 2006;37–40(195):5020–36.
[7] Hallquist J. Nike II: an implicit, finite deformation, finite element code for the analysing the static and dynamic response of two-dimensional solids. Report UCRL 52678. UC-Lawrence Livermore National Laboratory; 1979.
[8] Hill R. The mathematical theory of plasticity. Oxford: Clarendon Press; 1950.
[9] Kikuchi N, Oden JT. Contact problems in elasticity. Philadelphia: SIAM; 1988.
[10] Laursen TA. Computational contact and impactmechanics. Berlin, Heidelberg: Springer Verlag; 2002.
[11] Lubliner J. Plasticity theory. London: Macillan; 1990.
[12] Luenberger DG. Linear and nonlinear programming. Reading: Addison-Wesley; 1984.
[13] Prager W. Einführung in die Kontinuumsmechanik. Basel, Stuttgart: Birkäuser; 1961.
[14] Puso MA, Laursen TA. Mesh tying on curved interfaces in 3D. Eng Comput 2003;20(3):305–19.

[15] Sheng D, Eigenbrod P, Wriggers P. Finite element analysis of pile installation using large slip frictional contact. Comput Geotech 2005;32:17–26.
[16] Sheng D, Wriggers P, Sloan SW. Numerical algorithms for frictional contact in pile penetration analysis. Comput Geotech 2006;33(6–7): 341–54.
[17] Simo JC, Meschke G. A new class of algorithms for classical plasticity extended to finite strains: Application to geomaterials. Comput Mech 1993;11(4):253–78.
[18] Wriggers P. Finite element algorithm for contact problems. Arch Comp Meth Engng 1995;2(4):1–49.
[19] Wriggers P. Computational contact mechanics. first ed. John Wiley & Sons Ltd.; 2002. p. 306–09.
[20] Wriggers P. Computational contact mechanics. 2nd ed. Heidelberg: Springer-Verlag; 2006.
[21] Wriggers P, Krstulovic-Opara L. The moving friction cone approach for three-dimensional contact simulations. Int J Comput Methods 2004;1:105–19.
[23] Wriggers P, Simo JC. A note on tangent stiffness for fully nonlinear contact problems. Comput Appl Num Meth 1985;1: 199–203.